Structure-Dependent Hydrostatic Deformation Potentials of Individual Single-Walled Carbon Nanotubes

J. Wu,[1] W. Walukiewicz,[1] W. Shan,[1] E. Bourret-Courchesne,[1] J.W. Ager III,[1] K. M. Yu,[1] E. E. Haller,[1,2] Kyle Kissell,[3] Sergei M. Bachilo,[3] R. Bruce Weisman,[3] and Richard E. Smalley[3]

[1]*Materials Sciences Division, Lawrence Berkeley National Laboratory, Berkeley, California 94720, USA*
[2]*Department of Materials Science and Engineering, University of California, Berkeley, California 94720, USA*
[3]*Department of Chemistry, Rice University, 6100 Main Street, Houston, Texas 77005, USA*

(Received 11 November 2003; published 1 July 2004)

The hydrostatic pressure coefficients of interband transition energies of a number of single-walled carbon nanotubes with different chiralities were measured. Optical experiments were performed on debundled, single-walled carbon nanotube suspensions with hydrostatic pressure applied by diamond anvil cells. The pressure coefficients of the band-gap energies are negative and dependent on the nanotube structure, while the second van Hove transitions are much less sensitive to hydrostatic pressure. An empirical equation that relates the pressure coefficients to nanotube structure is presented and discussed.

DOI: 10.1103/PhysRevLett.93.017404 PACS numbers: 78.67.Ch, 62.25.+g, 71.20.Tx, 81.07.De

The unique electronic and mechanical properties and the prospects for technological applications of single-walled carbon nanotubes (SWNTs) have led to considerable research interest. Nanotubes can be either metallic or semiconducting, depending on their chiral structure, which is indexed by two integers (n, m) [1]. SWNTs have also been shown to have superior elastic properties that can accommodate large mechanical strains [2]. A more detailed understanding of the electromechanical responses of SWNTs is important in view of the practical manipulation of SWNTs. It has been predicted theoretically that under uniaxial stretch the band gap of a semiconducting SWNT should increase or decrease depending on whether $(n - m)$mod3 (the remainder of dividing $n - m$ by 3) is equal to 1 or 2 [3]. Experimental results have been shown to be consistent with these predictions [4,5]. For example, by measuring the conductance of SWNTs, Minot *et al.* found that their band gap is modulated by the axial tensile strain introduced by pushing the middle of a suspended nanotube with an atomic force microscope (AFM) tip [4]. However, all of these studies have been based on uniaxial tensile deformation along the tube axis. They have neglected the local distortion of the nanotubes by the touch of the AFM tip or the electrodes and have assumed a simultaneous contraction in the tube radial direction in accord with the Poisson's ratio [4,5]. Experimental investigations of SWNTs under uniform *hydrostatic* pressure have been limited to bundled nanotube ropes [6,7]. In these studies, the detected signals include not only contributions from the intrinsic response of individual nanotubes but also contributions from the intertube interactions within a bundle that are enhanced under pressure. These intertube interactions can cause considerable extrinsic, anisotropic effects on the individual nanotubes such as a polygonization of the tube cross section [7].

In general, bundled SWNTs do not fluoresce. Very recently, bright band-edge fluorescence has been observed from semiconducting SWNTs suspended by aqueous sodium dodecyl sulfate (SDS) surfactant in deuterium oxide (D_2O) and treated by intensive ultrasonication and subsequent centrifugation [8]. The resultant suspension is rich in dispersed individual SWNTs that are in van der Waals contact with the surrounding SDS surfactant coating, which is presumed to reduce the fluorescence quenching effects by isolating semiconducting nanotubes from metallic ones. This technique provides a unique way to study the intrinsic hydrostatic pressure behavior of *individual* nanotubes by optical spectroscopies. In this Letter, we present our systematic measurements of the hydrostatic pressure dependence of optical transitions in individual SWNTs. The deformation potentials of nanotube band gaps are derived within an elastic model. The pressure coefficients for different nanotube structures can be expressed as the summation of a diameter-dependent term and a chiral angle-dependent term.

A nanotube suspension containing 25.2 mg/l of SWNTs grown in high-pressure carbon monoxide was processed in a similar way as described in Ref. [8]. The optical absorption measurements were performed at room temperature using a halogen tungsten lamp dispersed by a 0.5 m monochromator as the light source. A Ge photodiode was used as the detector in the spectral range below 1.4 eV, and an ultraviolet-enhanced Si photodiode was used for energies above 1.4 eV. For pressure-dependent optical experiments, a drop of nanotube suspension was sealed in a gasketed diamond anvil cell for the application of hydrostatic pressure. The pressurized volume was a cylindrical-shaped hole (diameter $\sim$150 μm and length $\sim$200 μm) drilled into the spring steel gasket sheet. A small grain of ruby (~ 10 μm grain size) was also loaded in the volume. The applied pressure was calibrated

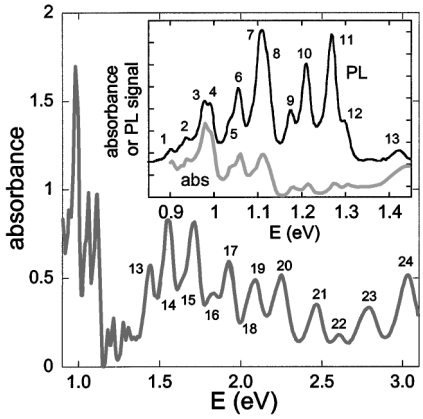

FIG. 1. Absorption spectrum of a SWNT suspension. The inset shows the absorption spectrum in the near infrared region in comparison with a PL spectrum. No PL peak was observed above 1.5 eV (not shown here). The peaks are numbered in order of increasing peak energy.

by the standard method of monitoring the redshift of the ruby R1 emission line.

Figure 1 shows the ambient-pressure absorption spectrum of the sample obtained on a CARY-2390 NIR-VIS-UV spectrophotometer after the featureless background baseline had been subtracted. A series of absorption peaks, similar to those reported in Ref. [8], are resolved distinctly. The peaks can be divided into two groups. In the energy region below $\sim$1.4 eV, 12 absorption peaks (group *A* transitions) are observed with full width at half maximum (FWHM) between 10 and 30 meV. In the energy region between 1.4 and 3.1 eV, there is another set of 12 peaks (group *B* transitions) with FWHM between 50 and 100 meV. For convenience of discussion, we number these peaks in the order of increasing peak energy (0.899 to 3.030 eV), as shown in Fig. 1. In addition to the difference of peak width, these two groups of transitions also exhibit completely different emission behavior. As is seen in the inset in Fig. 1, photoexcitation of the sample results in strong emission in the spectral range of the group *A* transitions, with each photoluminescence (PL) peak position well matched to an individual absorption peak [9]. In contrast, in the spectral range of group *B* transitions, no characteristic emission was detected (data not shown here).

The different characteristics between group *A* and group *B* are attributed to the different nature of optical transitions involved [10]. Group *A* peaks correspond to optical transitions across the band gap of the semiconducting nanotubes between the lowest unoccupied van Hove singularity (VHS) and the highest occupied VHS and are conventionally denoted as E_{11}. Group *B* peaks (E_{22}) are attributed to the transitions between the second pair of VHS above and below the Fermi level, respectively. Similar clustering and attribution of absorption peaks have also been discussed in Ref. [11].

Using an excitation-emission spectrofluoimetric mapping, Bachilo *et al.* have assigned each optical transition to a specific SWNT structure [10]. Using the empirical equation presented in Ref. [10], we have assigned a pair of (n, m) structure indices to each peak in group *A* and group *B*. The assignment is listed in Table I. Peaks 18, 21, 22, and 23 do not match any E_{11} peaks observed in the range. They are attributed to the lowest-energy van Hove transitions of metallic nanotubes in the sample [10].

The effect of hydrostatic pressure on the absorption spectrum of group *A* peaks is shown in Fig. 2(a). All peaks shift to lower energy with increasing hydrostatic pressure, opposite to most conventional direct-gap semiconductors. The width, line shape, and intensity of all peaks are well maintained from that at ambient pressure up to 8.5 kbar, at which the peaks start to weaken and broaden. At pressures above $\sim$11 kbar, the sample turns

TABLE I. Absorption peak energies, linear pressure coefficients, deformation potentials, and corresponding nanotube assignments.

E_{11} peak	E_{11} (eV)	dE_{11}/dP (meV/kbar)	$dE_{11}/d\ln V$ (eV)	Assignment (n, m)	E_{22} peak	E_{22} (eV)	dE_{22}/dP (meV/kbar)
1	0.899			(9, 8)	14	1.543	−0.3
2	0.933			(12, 2)	16	1.828	
3	0.977	−2.9	6.4	(8, 7)	15	1.700	−1.3
4	0.994			(11, 1)	19	2.083	−0.7
5	1.035	−4.6	10.3	(11, 3)	14		
6	1.054	−3.0	7.0	(8, 6)	15		
7	1.105	−2.0	4.9	(7, 6)	17	1.917	−1.6
8	1.123			(9.4)	15		
9	1.173	−3.8	9.5	(10, 2)	15		
10	1.209	−1.8	4.7	(7, 5)	17		
11	1.272	−1.0	2.8	(6, 5)	20	2.239	−0.4
12	1.295			(8, 3)	17		
13	1.428	−0.6	2.1	(6, 2)	24	3.030	

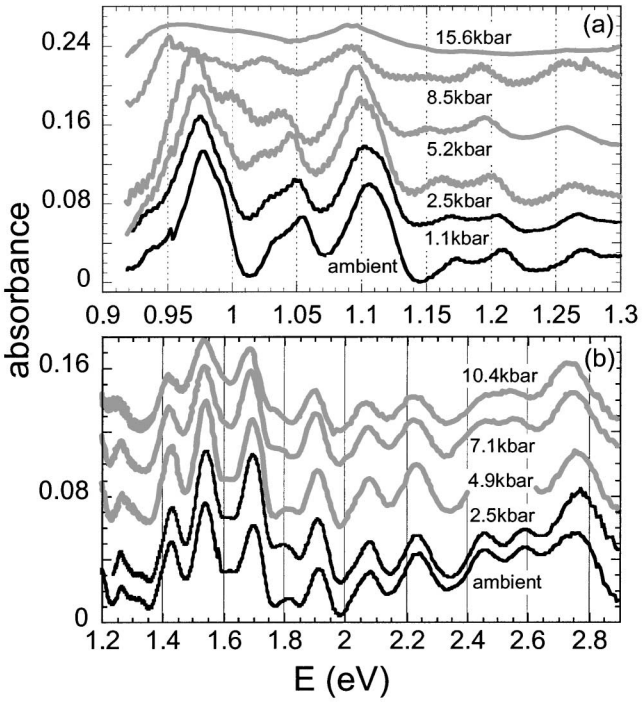

FIG. 2. (a) Absorption spectrum in the near infrared (group *A*) taken at a range of hydrostatic pressures. The curves are vertically offset for clarity. (b) Absorption curves at higher energies (group *B*) as a function of pressure.

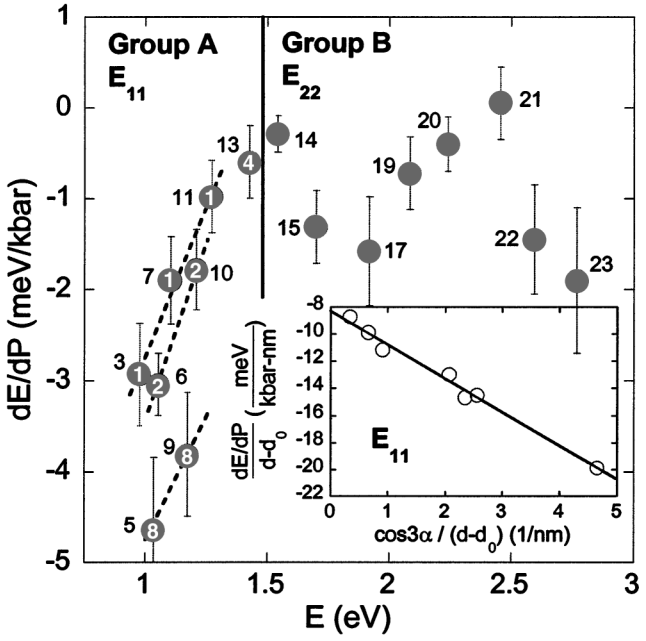

FIG. 3. Measured linear pressure coefficients as a function of peak energy. The number beside each data point shows the peak number. Numbers in the E_{11} symbols are the value of $n - m$. The dashed lines connect families with equal $n - m$ values. The inset shows the dependence given by Eq. (1) for all E_{11} points.

from a homogenous liquid into a multigrain-structured phase, and the resultant light scattering severely reduces the optical signal. This phase transition is related to the well-known crystallization of D_2O into a tetragonal solid phase (water VI) at 11 kbar at room temperature. Similar to the pressure dependence of absorption, the E_{11} PL peaks also shift to lower energy under pressure (not shown here). The PL peak and the corresponding absorption peak show very similar pressure dependence. In Fig. 2(b) we show the absorption spectrum of the group *B* transitions under various hydrostatic pressures. Unlike the group *A* absorption peaks, most of the group *B* peaks shift only slightly to lower energy. The pressure coefficient of each peak is obtained from a least-square linear fitting to the pressure dependence of the absorption peak, which is shown in Fig. 3 and listed in Table I.

A few conclusions can be drawn from the results in Fig. 3. First of all, the application of hydrostatic pressure to SWNTs always decreases the band gap (E_{11}) irrespective of whether the value of $q = (n - m)\mathrm{mod}3$ is equal to 1 or 2. This behavior is in contrast to the effects of uniaxial stress where both decrease and increase of the band gap are possible depending on the value of q [4,5]. The pressure coefficients for E_{22} transitions are considerably smaller than those of E_{11} transitions. We note that a similar, overall shift to lower energy (~ -2 meV/kbar below 10 kbar) of a broad absorption peak under hydrostatic pressure has been reported on *bundled* nanotubes [6]. Our studies show that the negative pressure coefficient is an intrinsic property of *individual* nanotubes, rather than an effect of intertube interactions within a bundle under high pressures.

Because of the highly anisotropic geometry of nanotubes, their mechanical properties are different in the axial direction and the radial direction. By performing first-principles calculations of the elastic constants of individual nanotubes, Reich *et al.* have found that the linear moduli are insensitive to chirality for nanotubes with the same diameter. They have introduced a continuum model within classical elasticity theory to model the bulk modulus ($dP/d\ln V$) of SWNTs [12]. We have calculated the hydrostatic deformation potential of the nanotube band gap from $dE_{11}/d\ln V = (dE_{11}/dP)(dP/d\ln V)$ and the calculated results are listed in Table I. The magnitude of deformation potentials is smaller than that of diamond (25 eV), but comparable to that of most other compound semiconductors.

Another striking effect shown in Fig. 3 is that the magnitude of pressure coefficients of the group *A* peaks ($|dE_{11}/dP|$) tends to increase with decreasing transition energy. Since the main term in E_{11} is inversely proportional to the tube diameter, this leads to the conclusion that the electronic states of larger-diameter nanotubes are more sensitive to hydrostatic pressure. In addition to this general trend, Fig. 3 also shows a pattern of larger $|dE_{11}/dP|$ for nanotubes with larger $n - m$ values. A

very similar pattern of family grouping has been observed in the transition energies plot [10]. This pattern signifies a chiral angle (α) dependence in addition to the diameter (d) dependence. We found that the pressure coefficient for all the E_{11} data can be well described by the following equation:

$$\frac{dE_{11}}{dP} = a(d - d_0) + b\cos 3\alpha, \quad (1)$$

where $a = -8.3$ meV/(kbar nm), $d_0 = 0.68$ nm [13], and $b = -2.5$ meV/kbar. In the inset in Fig. 3, the straight line represents the dependence given by Eq. (1). The first term, which is linear in diameter, is related to the fact that the radial compression induced by external pressure is one phase of the nanotube's radial breathing vibrational phonon mode. This mode is experimentally visible in Raman spectra because it has an unusually large resonant intensity enhancement as a result of its strong coupling to electronic excitations from valence to conduction bands [14,15].

Tight binding calculation based on the graphene π-electron model has shown that the band gap of a radially deformed SWNT should increase or decrease depending on the relative shift of the Fermi wave vector with respect to the nearest **k** line in the tube circumferential direction [3]. Therefore, the overall negative pressure coefficient that we observed is likely a higher-order effect beyond the graphene π-electron model. One possible mechanism that could account for the negative pressure coefficients is the σ^*-π^* hybridization effect occurring near the large curvature points of nanotubes [16]. It has been demonstrated that the rehybridization between singlet σ^* and π^* conduction bands results in a drastic downward shift of the lowest conduction band in small-diameter nanotubes [16] or radially deformed nanotubes [17]. The hybridization effect is the strongest in zigzag nanotubes where $\alpha = 0$ and vanished in armchair nanotubes where $\alpha = 30°$ [17,18]. The second lowest conduction band, which is responsible for the E_{22} transitions, is less sensitive to the σ^*-π^* hybridization [17]. These are consistent with the α dependence of $|dE_{11}/dP|$ in Eq. (1) and the insensitivity of the E_{22} peaks to hydrostatic pressure, as is shown in Fig. 3. A quantitative explanation of the observed negative and patterned hydrostatic pressure coefficients of SWNT band gaps requires further theoretical exploration.

We thank Professor S. G. Louie and Professor R. B. Capaz for helpful discussions. This work was supported by the Director, Office of Science, Office of Basic Energy Sciences, Division of Materials Sciences and Engineering, of the U.S. Department of Energy under Contract No. DE-AC03-76SF00098. R. B. W. and S. M. B. gratefully acknowledge support from the National Science Foundation (Grant No. CHE-0314270) and the Welch Foundation (Grant No. C-0807).

[1] R. Saito, G. Dresselhaus, and M. S. Dresselhaus, *Physical Properties of Carbon Nanotubes* (Imperial College, Singapore, 1998).
[2] J. P. Salvetat, J. M. Bonard, N. H. Thomson, A. J. Kulik, L. Forro, W. Benoit, and L. Zuppiroli, Appl. Phys. A **69**, 255 (1999).
[3] Liu Yang and Jie Han, Phys. Rev. Lett. **85**, 154 (2000).
[4] E. D. Minot, Yuval Yaish, Vera Sazonova, Ji-Yong Park, Markus Brink, and Paul L. McEuen, Phys. Rev. Lett. **90**, 156401 (2003).
[5] J. Cao, Q. Wang, and H. Dai, Phys. Rev. Lett. **90**, 157601 (2003).
[6] S. Kazaoui, N. Minami, H. Yamawaki, K. Aoki, H. Kataura, and Y. Achiba, Phys. Rev. B **62**, 1643 (2000).
[7] J. Tang, L. Qin, T. Sasaki, M. Yudasaka, A. Matsushita, and S. Iijima, Phys. Rev. Lett. **85**, 1887 (2000).
[8] M. J. O'Connell, S. M. Bachilo, C. B. Huffman, V. C. Moore, M. S. Strano, E. H. Haroz, K. L. Rialon, P. J. Boul, W. H. Noon, C. Kittrell, J. Ma, R. H. Hauge, R. B. Weisman, and R. E. Smalley, Science **297**, 593 (2002).
[9] Absorption Peak-13 (1.428 eV; width ~40 meV) is on the border between group *B* and group *A*. Since a weak PL peak is also observed near this energy (see inset in Fig. 1), we tentatively place Peak-13 in group *A*.
[10] S. M. Bachilo, M. S. Strano, C. Kittrell, R. H. Hauge, R. E. Smalley, and R. B. Weisman, Science **298**, 2361 (2002).
[11] A. Hagen and T. Hertel, Nano Lett. **3**, 383 (2003).
[12] S. Reich, C. Thomsen, and P. Ordejon, Phys. Rev. B **65**, 153407 (2002).
[13] We note that the value of d_0 is close to 2 times the wall thickness.
[14] A. M. Rao *et al.*, Science **275**, 187 (1997).
[15] M. A. Pimenta *et al.*, J. Mater. Res. **13**, 2396 (1998).
[16] X. Blase, L. X. Benedict, E. L. Shirley, and S. G. Louie, Phys. Rev. Lett. **72**, 1878 (1994).
[17] J. C. Charlier, Ph. Lambin, and T. W. Ebbesen, Phys. Rev. B **54**, 8377 (1996).
[18] A. Kleiner and S. Eggert, Phys. Rev. B **64**, 113402 (2001).